Bioconjugate Chemistry

Article

Cite This: *Bioconjugate Chem.* 2019, 30, 959−965

pubs.acs.org/bc

Selective Labeling and Decoration of the Ends and Sidewalls of Single-Walled Carbon Nanotubes Using Mono- and Bispecific Solid-Binding Fluorescent Proteins

Sonja J.G. Dunakey, Brandon L. Coyle, Alexander Thomas, Meng Xu, Brian J.F. Swift, and François Baneyx*

Department of Chemical Engineering, University of Washington, Box 351750, Seattle, Washington 98195, United States

Supporting Information

ABSTRACT: Simple and robust strategies for the noncovalent functionalization of carbon nanostructures with proteins are of considerable interest in hybrid nanomaterials synthesis, part-to-part assembly, and biosensor development. Here, we show that fusion of the Car9 and Car15 carbon-binding peptides to the C-termini of the sfGFP and mCherry fluorescent proteins enables selective labeling of the ends or the sidewalls of single walled carbon nanotubes. By installing a gold-binding peptide or a single cysteine residue in carbon-binding variants of sfGFP, we further produce heterobifunctional solid-binding proteins that support the decoration of nanotubes sidewalls or termini with gold nanoparticles. The approach described here is generic and should prove useful for the controlled assembly of other hybrid materials.

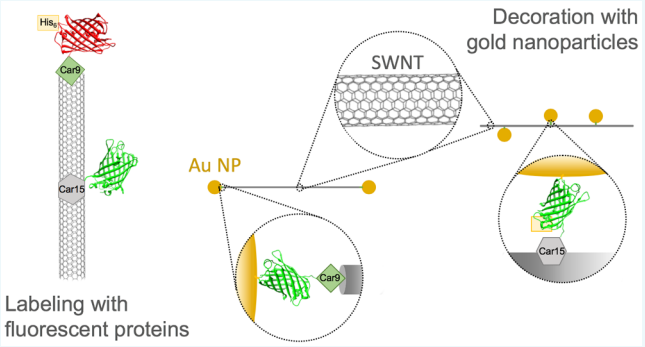

INTRODUCTION

Carbon nanotubes (CNTs) have attracted considerable attention for the fabrication of composite and hybrid materials due to their exceptional mechanical and electrical properties.[1−3] They can be found as single-walled (SWNT) or multiwalled (MWNT) structures and exhibit metallic or semiconducting properties depending on how the sp^2-hybridized carbon lattice aligns with the nanotube axis.[2] Semiconducting SWNT are of particular interest for biosensor development,[4−6] as their conductivity is highly sensitive to the local environment, their response is fast, and the detection area is scalable to the size of individual proteins.[7−9] However, they are difficult to manipulate in aqueous solutions because high hydrophobicity leads to bundling and aggregation.[10] While the issue can been addressed by oxidizing the carbon lattice with acids to form solubilizing hydroxyl and carboxyl surface groups suitable for protein conjugation to the nanotube surface,[10] acid treatment degrades electrical properties.[11] This limitation has triggered an interest in the development of noncovalent strategies for functionalizing nanotubes with proteins.[12]

The simplest approach, nonspecific adsorption, does not provide for orientation control and can be accompanied by protein unfolding at the hydrophobic carbon interface.[7,13−15] Amphiphilic polymers (e.g., polyethylene glycol modified with pyrene groups and polystyrene-*block*-poly(acrylic acid))[10,16] and surfactants (e.g., sodium cholate, sodium dodecyl sulfate, and Triton)[10,17−20] have also been used as solubilizing agents. Here, hydrophobic domains bind nonspecifically to the nanotube sidewalls while hydrophilic regions support dispersion in aqueous solvents and provide a functional handle for protein conjugation.[20−22] While these methods work well, they require multiple steps to yield the desired product.

Solid binding peptides (SBPs)[23] selected by phage or cell surface display for their ability to bind various forms of carbon[24−28] have also been used for CNT solubilization and manipulation. They offer the advantage of one-step conjugation and provide an opportunity to build more complex nanotube-based structures. For instance, heterofunctional polypeptides have been used to precipitate titania and silica on SWNT[25,29] and to decorate thin nanotube films with evenly spaced gold nanoparticles.[14] However, like detergents and polymers, synthetic polypeptides tend to wrap around the nanotubes, limiting the number of accessible architectures and conjugation chemistries.

Previously, we reported that the Car9 (DSARGFKKPGKR) and Car15 (RTYLPLPWMAAL) SBPs exhibit distinct carbon-binding modalities.[30] The more hydrophobic Car15 preferentially binds to sp^2- over sp^3-hybridized carbon, while Car9, which is rich in positively charged residues favors the carbonyl, carboxyl, and hydroxyl-rich edges of highly oriented pyrolytic graphite (HOPG) and glassy carbon.[30] Consistent with these observations, Car9 was later found to bind to silanol-rich silica

Received: February 4, 2019
Revised: February 26, 2019
Published: February 28, 2019

DOI: 10.1021/acs.bioconjchem.9b00097
Bioconjugate Chem. 2019, 30, 959−965

surfaces, enabling oriented immobilization,[31] controlled protein release,[32] and affinity purification[33,34] of Car9-tagged fusion proteins using inexpensive silica substrates.

Because the sidewalls of CNTs primarily consist of sp^2-hybridized carbon, while their ends are sp^3-like with significant defects in the carbon lattice and numerous free hydroxyl and carboxyl groups,[10] we explored the possibility of using Car15- and Car9 for the single-step, noncovalent conjugation of proteins to nanotubes ends and sidewalls. We describe here Car9- and Car15-based fluorescent carbon-binding proteins that achieve this goal and further engineer these solid binding proteins to orchestrate the formation of hybrid nanostructures in which gold nanoparticles are selectively coupled to SWNTs walls or termini.

RESULTS AND DISCUSSION

Selective Labeling of the Sidewalls and Ends of Carbon Nanotubes with Carbon-Binding Fluorescent Proteins. To facilitate the visualization of carbon binding proteins, we genetically appended the Car15 sequence to the C-terminus of the thermodynamically stable superfolder green fluorescent protein (sfGFP)[35] and fused Car9 to the C-terminus of a monomeric version of the *Dicosoma* red fluorescent protein fitted with a N-terminal hexahistidine tag (His-mCherry).[36] A GGGS linker between native C-termini and SBPs imparted conformational flexibility and served as a spacer to separate fluorescent proteins from the hydrophobic, and potentially denaturing, carbon nanotube surface (Figure 1A).

To determine if the resulting fusion proteins would support solubilization and selective labeling of nanotubes from the dry state, SWNT powder was taken in a solution of sfGFP-Car15, subjected to sonication, and further incubated with His-mCherry-Car9 (Figure 1A). Fluorescence imaging in the GFP emission window revealed elongated features consistent with the labeling of the nanotubes' sidewalls by sfGFP-Car15 (Figure 1B). Because wild-type sfGFP does not support nanotube dispersion under the same experimental conditions, sfGFP-Car15 is likely to exert its solubilizing effect by binding to the walls of SWNT at multiple locations, as schematically depicted in Figure 1A. A small number of discrete fluorescent spots were observed when 587 nm light was used to excite mCherry (Figure 1C). Some of this punctuated red fluorescence was connected to the zones of GFP labeling in merged images (Figure 1D), suggesting that His-mCherry-Car9 occasionally binds to the ends of sfGFP-Car15-solubilized SWNTs as illustrated in Figure 1A. However, the process was inefficient, and although care was taken to minimize sonication time (a minimum of 3 min of sonication at a power of 12 W was needed to produce a colloidal solution that withstood centrifugation at 12 000*g*), we observed significant nanotube shortening (Figure 1B) in good agreement with other published reports.[37,38] We therefore turned our attention to a gentler, dialysis-based approach.

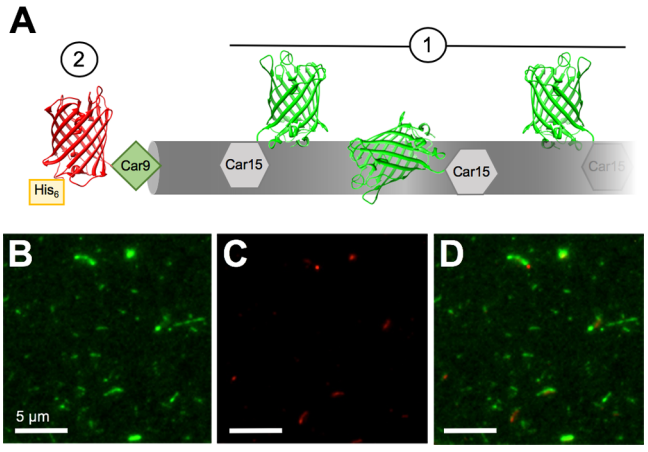

Figure 1. Selective labeling of SWNT with carbon-binding fluorescent proteins through sonication. (A) Schematic representation of the binding of His-mCherry-Car9 and sfGFP-Car15 to SWNT. The Car9 SBP is depicted by a green diamond, Car15 by a gray hexagon, and the hexahistidine tag by a yellow rectangle. Binding of sfGFP-Car15 to the sidewalls of SWNT upon sonication in buffer containing 1 μM of protein enables nanotube solubilization (step 1). Some of the nanotubes ends are bound upon addition of 0.5 μM His-mCherry-Car9 (step 2). Fluorescence microscopy images were collected under 473 nm (B) or 587 nm excitation (C) to visualize sfGFP and mCherry, respectively. (D) Merged image. An average length of 1 μm is specified by the manufacturer.

Both charged (e.g., sodium cholate and sodium dodecyl sulfate) and neutral surfactants (e.g., Triton) have long been used to improve the dispersion of carbon nanotubes in aqueous solvents.[10,17,18,20] To determine if efficient and specific nanotube labeling could be achieved by exchanging stabilizing surfactant molecules for carbon-binding proteins, we purchased colloidal suspensions of semiconducting SWNT, diluted the proprietary mixture of stabilizing detergents with sodium cholate, and performed extensive dialysis in the presence of Car9- and Car15-tagged proteins.

For these experiments, we swapped the carbon-binding sequences at the C-termini of sfGFP and mCherry (Figures 2A and B) to allow for removal of unbound proteins through two orthogonal affinity purification steps performed at the conclusion of ligand exchange. Ni-NTA agarose[39] was used to capture and preferentially remove any His-mCherry-Car15 whose hexahistidine tag was freely accessible (e.g., not sequestered in the vicinity of the nanotube surface by the binding of the Car15 extension to SWNT sidewalls). Silica affinity chromatography[33] was used to capture any free sfGFP-Car9 that was not bound to the end of SWNTs through its Car9 extension. This operation not only improved image quality by removing background fluorescence but also enabled sequential labeling and decoration schemes (see below). However, while suspensions of sfGFP-Car9- and His-mCherry-Car15-decorated SWNT were stable for up to 8 weeks, removal of excess protein by affinity chromatography led to a decrease in colloidal stability with visible aggregates starting to form after 10 days.

Fluorescence microscopy imaging of protein-stabilized SWNT revealed punctuated features in the case of sfGFP-Car9 (Figure 2C) and more extended ones in the case of His-mCherry-Car15 (Figure 2D), consistent with binding to the ends and sidewalls of the nanotubes, respectively. In the case of sfGFP-Car9, fluorescent spots often appeared paired in sparsely populated fields (Figures 2C and D). Similar results were obtained with metallic SWNT (Figure S1A in Supporting Information). In both cases, separation distances between paired spots were in good agreement with the nanotube length distribution provided by the manufacturer (from 300 nm to 5 μm; Figure S2). By contrast, images of His-mCherry-Car15-stabilized SWNT showed clustered fluorescence with a high aspect ratio, as would be expected upon labeling of their

DOI: 10.1021/acs.bioconjchem.9b00097
Bioconjugate Chem. 2019, 30, 959−965

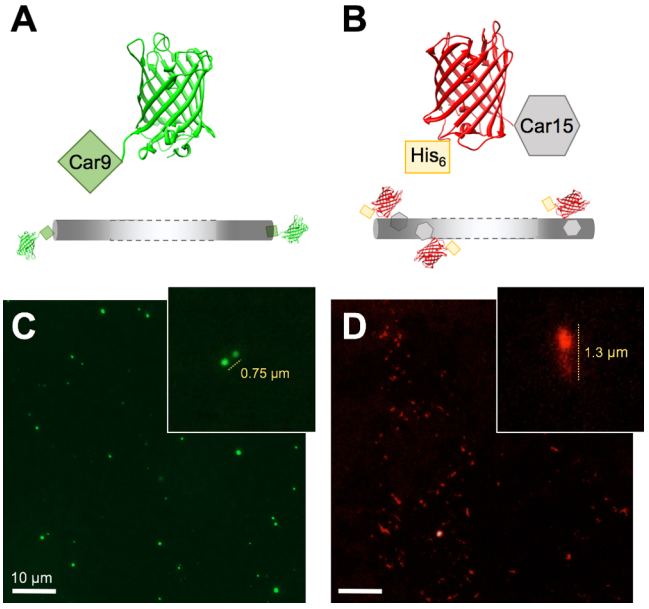

Figure 2. Selective labeling of SWNT with carbon-binding fluorescent proteins through ligand exchange. Schematic representations of sfGFP-Car9 (A) and His-mCherry-Car15 (B) and of their SWNT binding modalities. (C) Fluorescence microscopy image of semiconducting SWNT treated with sfGFP-Car9 under 473 nm excitation. The inset shows a magnified image in a sparsely populated region consistent with the labeling of both ends of a single SWNT. (D) Fluorescence microscopy image of semiconducting SWNT treated with His-mCherry-Car15 under 587 nm excitation. The inset image is consistent with sidewall labeling of a single SWNT.

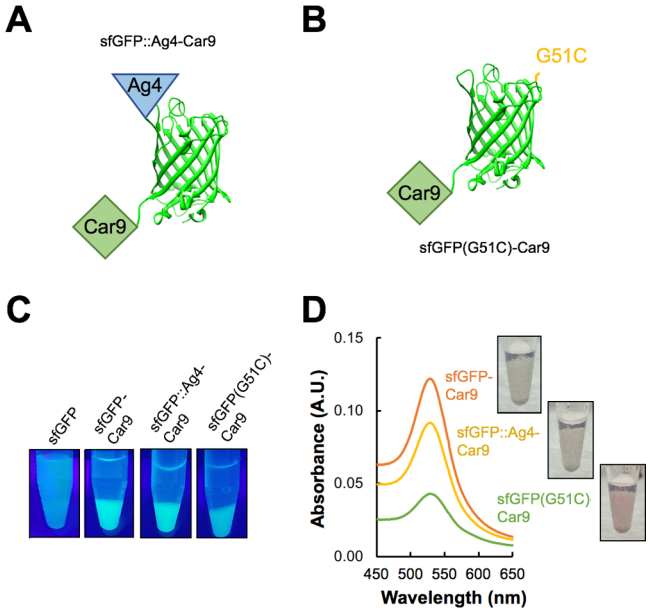

Figure 3. Construction of bifunctional fluorescent proteins for gold and nanotube end-binding. Schematic representations of sfGFP::Ag4-Car9 (A) and sfGFP(G51C)-Car9 (B). The Ag4 and Car9 SBPs are depicted as blue triangles and green diamonds, respectively. The G51C mutation is identified in yellow. (C) The Car9 SBP enables quantitative protein immobilization on silica beads and oriented presentation of the gold-binding moiety. (D) Cys51 is more effective than Ag4 at binding 50 nm diameter, citrate-capped gold nanoparticles as evidenced by lower gold colloid absorption in the supernatant and a pinker silica phase.

sidewalls (Figure 2D). Taken together with the data of Figure 1, these results indicate that Car9 extensions confer proteins to which they are fused an ability to solubilize carbon nanotubes by binding to their ends, while fused Car15 extensions perform a similar function by binding to nanotubes sidewalls.

Building Heterobifunctional Solid-Binding Proteins for Carbon- and Gold-Binding. To enable a long-term goal of using heterobifunctional solid-binding proteins to assemble carbon nanostructures on gold contacts for electronic device fabrication, we set out to combine nanotube end- and gold-binding functionalities on the same fluorescent protein scaffold. To this end, we engineered the Ag4 sequence (NPSSLFRYLPSD), an SBP that binds to both silver[40] and gold,[41] within permissive loop 9 of sfGFP-Car9,[42] which lies on the opposite side of the GFP β-barrel relative to the C-terminal Car9 extension (Figure 3A). As an alternative, we took advantage of the well-documented ability of cysteines to coordinate gold[43] by introducing the Gly51-Cys mutation within loop 3 of sfGFP-Car9, which is also permissive[35] and projects on the same side of the β-barrel as loop 9 (Figure 3B). The nearby Cys48 was converted to a serine to prevent the formation of an unwanted disulfide bond. The resulting proteins, sfGFP::Ag4-Car9 and sfGFP(G51C)-Car9, could be efficiently purified by silica affinity chromatography (Figure S3 in Supporting Information).

To demonstrate and quantify gold-binding activity, we first adsorbed the proteins to silica beads through their Car9 extension to orient the Ag4 sequence or Cys51 toward the bulk solution. As expected, all fluorescent material quantitatively partitioned with the silica phase (Figure 3C). Next, citrate-capped gold nanoparticles 50 nm in diameter were added, and the UV−visible spectra of the supernatants were recorded after 30 min of mixing. Comparison of absorption intensities at the plasmon peak (529 nm, Figure S4 in Supporting Information) revealed that whereas the Ag4 SBP endowed sfGFP-Car9 with the ability of capturing about 25% of the colloid relative to the control, immobilized sfGFP(G51C)-Car9 bound nearly 65% of the nanoparticles. The efficiency of protein-mediated partitioning of gold nanoparticles in the silica phase could be visually confirmed by a progressive increase in the pink color of the solid phase (Figure 3D). Thus, while both constructs are bifunctional, and for reasons that at present remain unclear, cysteine-mediated capture of 50 nm gold particles is much more efficient than their Ag4-mediated binding.

Informed by this result, we constructed a companion His-sfGFP(G51C)-Car15 protein that would combine nanotube sidewall- and gold-binding activities (Figure 4A). Bifunctionality was tested as above except that we took advantage of the N-terminal hexahistidine tag to achieve oriented immobilization of His-sfGFP(G51C)-Car15 (and the His-sfGFP-Car15 control protein) on Ni-NTA agarose beads. Interestingly, Ni-NTA agarose-conjugated His-sfGFP(G51C)-Car15 bound more colloidal gold (80%) than sfGFP(G51C)-Car9 immobilized on silica likely due differences in Cys51 presentation or matrix-related effects.

Solid-Binding Proteins-Mediated Decoration of SWNT with Gold Nanoparticles. We next set out to demonstrate that sfGFP(G51C)-Car9 and His-sfGFP(G51C)-Car15 would be suitable to control the assembly of gold nanoparticles onto SWNT templates. For these experiments, we first adsorbed carbon-binding proteins to the ends or sidewall of semiconducting nanotubes using the ligand

DOI: 10.1021/acs.bioconjchem.9b00097
Bioconjugate Chem. 2019, 30, 959−965

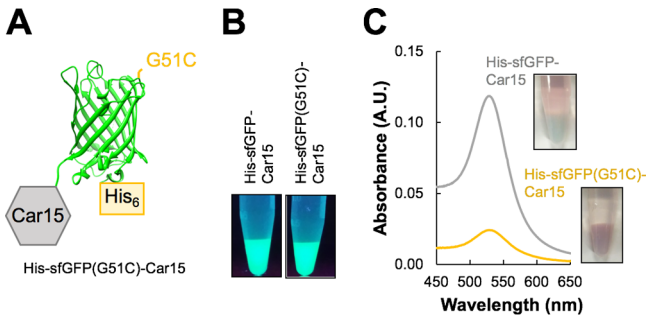

Figure 4. Construction of a bifunctional fluorescent protein for gold and nanotube sidewall-binding. (A) Schematic representations of His-sfGFP(G51C)-Car15. (B) The N-terminal hexahistidine tag enables quantitative protein immobilization on Ni-NTA agarose beads and oriented presentation of Cys51. (C) UV−visible absorption spectra of supernatants and appearance of the resin following incubation with 50 nm gold nanoparticles.

exchange strategy of Figure 2, incubated the conjugates with 50 nm gold nanoparticles, and imaged the samples by scanning electron microscopy (SEM). In agreement with the fluorescence microscopy data of Figure 3C, gold nanoparticles were typically found in pairs with average separation distances of 600 nm in the case of sfGFP(G51C)-Car9-treated SWNT (Figure 5A; also see Figure S5 in Supporting Information). Transmission electron microscopy (TEM) imaging confirmed the presence of nanoparticle−nanotube connections in these samples (Figure S6 in Supporting Information). On the other hand, gold particles were usually present in linear groupings of three or more with separation distances averaging 180 nm in SWNT samples derivatized with His-sfGFP(G51C)-Car15 (Figure 5B; also see Figure S7 in Supporting Information). Both behaviors were in sharp contrast with the random distribution and large separation distances (>2 μm) observed in the case of unconjugated gold nanoparticles (Figure S8 in Supporting Information). We conclude that sfGFP frameworks engineered with SBPs that specifically recognize the sidewalls (Car15) or ends (Car9) of SWNT along with oppositely located gold-binding functionalities are suitable to orchestrate the organization of gold nanoparticles on nanotube templates.

CONCLUSIONS

In this study, we showed that the Car9 and Car15 carbon binding peptides endow fluorescent proteins to which they are fused with the ability to selectively recognize the ends and sidewalls of SWNTs. By exploiting the host protein scaffold to display a carbon binding sequence together with a gold-binding peptide, or more effectively an engineered cysteine residue at well-defined spatial locations, we have further shown that it is possible to produce dual materials binders that support the selective conjugation of gold nanoparticles to the ends and sidewalls of SWNT. While nanotube sidewalls are not uniformly decorated, the approach is generic and should prove useful for biosensor development and the controlled assembly of other hybrid materials. It also holds promise for the creation of reconfigurable assemblies through the use of stimuli-responsive protein scaffolds.

EXPERIMENTAL SECTION

DNA Manipulations and Protein Purification. All plasmids were constructed using standard molecular biological approaches and verified by DNA sequencing. Proteins were purified by ion exchange chromatography (sfGFP-Car15 and His-mCherry-Car9), silica affinity chromatography (sfGFP-Car9, sfGFP::Ag4-Car9, and sfGFP(G51C)-Car9) or Ni-NTA chromatography (His-mCherry-Car15, His-mCherry-Car9, His-sfGFP-Car15, and His-sfGFP(G51C)-Car15). Detailed protocols are provided in the Supporting Information.

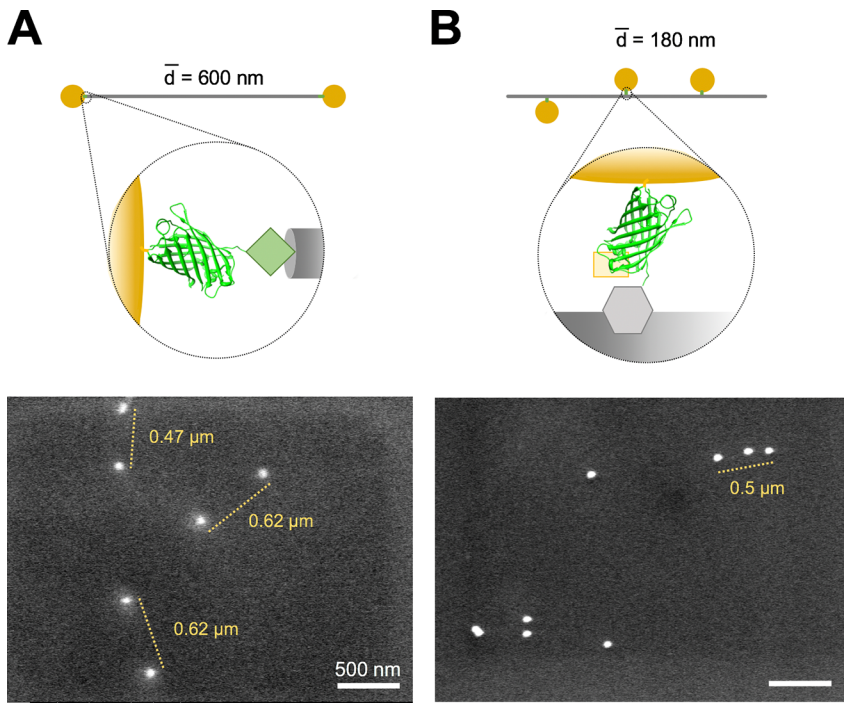

Figure 5. Schematic depiction and SEM images of the coupling of 50 nm gold nanoparticles to the ends (A) or sidewalls (B) of semiconducting SWNT through the use of sfGFP(G51C)-Car9 (A) or His-sfGFP(G51C)-Car15 (B).

DOI: 10.1021/acs.bioconjchem.9b00097
Bioconjugate Chem. 2019, 30, 959−965

Carbon Nanotubes Resuspension. For sonication-mediated solubilization, approximately 1 mg of dry SWNT (Sigma-Aldrich 775533, median length 1 μm, average diameter 0.84 nm, and 95% pure) were transferred to a 5 mL glass vial containing 2.7 mL of 50 mM phosphate buffer pH 7.5. The mixture was sonicated for 1.5 min on a Branson Sonifier 450 operated at 12W and 100% duty cycle using a microtipped wand. Next, 300 μL of phosphate buffer containing 10 μM sfGFP-Car15 and 5 μM His-mCherry-Car9 was added, and the solution was sonicated as above for another 3 min. Vials were immersed in a mixture of EtOH and ice to minimize heat-induced protein denaturation. Samples were centrifuged at 14 000*g* for 15 min to remove insoluble material and imaged by fluorescence microscopy.

Solutions of metallic and semiconducting SWNT (0.01 mg/mL, 300 nm to 5 μm in length, 1.2 to 1.7 nm in diameter with a mean diameter of 1.4 nm, and 90% pure) were purchased from NanoIntegris (Boisbriand, Quebec, Canada). The proprietary combination of detergents stabilizing the nanotubes was replaced with sodium cholate by mixing 750 μL of colloidal solution with 750 μL of 2 wt % Na-Cholate in 20 mM of Tris-HCl pH 7.5 (Buffer A) and agitating the mixture for 20 min at 21 °C. Proteins (400 μL of 10 μM stock solutions) were added, and mixing continued for 20 min. The solution was transferred to 10 000 MWCO dialysis tubing and dialyzed for 36 h at 10 °C against 0.5 L Buffer A with buffer exchange at 12 and 24 h. The final concentrations of SWNT and protein (bound and free) were 0.004 mg/mL and 2 μM, respectively, with slight variations associated with volume change during dialysis.

Fluorescence Microscopy. Protein−nanotube conjugates were imaged on a Nikon Eclipse fluorescence microscope at 90× magnification. Samples prepared by sonication were diluted fourfold with 50 mM phosphate buffer pH 7.5 and 10 μL aliquots were imaged as described below. Samples prepared by ligand exchange (100 μL) were first incubated for 10 min and without agitation with either 10 μL of silica (Davisil 643, Sigma) for Car9-tagged proteins or 10 μL of HisPur Ni-NTA (Thermo Scientific) for His-tagged variants to remove unbound proteins. Both matrixes were first equilibrated in Buffer A before use. Aliquots (10 μL) were imaged by fluorescence microscopy with illumination through a 480/40 nm wavelength filter (for sfGFP) or a 520/40 nm wavelength filter (for mCherry)., and fluorescence was collected in the 510−560 or 600−660 nm windows for sfGFP and mCherry derivatives, respectively.

Gold Nanoparticle−Protein Interactions. Citrate-capped gold nanoparticles 50 nm in diameter (NanoXact Gold #DAC1278) in 2 mM sodium citrate and at the manufacturer's specified concentration of 0.05 mg/mL (calculated to be 6.6×10^{-5} μM using a density of 19.32 g/cm^3 for 50 nm gold nanoparticles) were purchased from NanoComposix (San Diego, CA). To test the ability of Car9-tagged proteins to bind to gold, 1 mL of 0.5 μM sfGFP-Car9, sfGFP::Ag4-Car9, or sfGFP(G51C)-Car9 in Buffer A were added to 200 μL of Davisil grade 646 silica (Sigma) that had been washed with Buffer A. After 3 min of incubation with gentle agitation, gold nanoparticles (100 μL) were added, and the mixture was mixed for an additional 30 min at room temperature. UV−visible spectra of 1 mL of supernatant were collected after the silica had settled (2−3 min). The ability of Car15-tagged proteins to bind to gold was tested as above except that 1 mL of 0.5 μM of His-sfGFP-Car15 or His-sfGFP(G51C)-Car15 was added to 100 μL of Ni-NTA slurry (HisPur Ni-NTA, Thermo Scientific) that had been washed with Buffer A.

Scanning Electron Microscopy. Protein-stabilized SWNT (80 μL) prepared by ligand exchange were mixed with 20 μL of gold nanoparticles for 30 min at room temperature on a rotary mixer operated at 60 rpm. Aliquots (30 μL) were deposited on a silicon wafer and allowed to stand at room temperature for 5 min. Excess moisture was wicked away with filter paper and the wafer was washed 4 times with ddH_2O water by dunking, and wicking away excess liquid between each washing step. Wafers were allowed to dry overnight on filter paper in a Petri dish placed in a fume hood and samples were imaged on a FEI Sirion XL30 scanning electron microscope at an accelerating voltage of 5 kV.

■ ASSOCIATED CONTENT

Supporting Information

The Supporting Information is available free of charge on the ACS Publications website at DOI: 10.1021/acs.bioconjchem.9b00097.

Fluorescence microscopy image of metallic SWNT resuspended with sfGFP-Car9, distribution of distances between paired fluorescence spots for semiconducting and metallic SWNT end-decorated with sfGFP-Car9, SDS-PAGE analysis of purified proteins used in this study, UV−visible absorption spectrum of gold nanoparticles, additional SEM images of SWNT whose ends are decorated with sfGFP(G51C)-Car9 and gold nanoparticles, TEM image and schematic representation of a ca. 50 nm gold nanoparticle coupled to a ∼1.5 nm semiconducting SWNT, additional SEM images of SWNT whose sidewalls are decorated with His-sfGFP-(G51C)-Car15 and gold nanoparticles, SEM images of 50 nm gold nanoparticles in the absence of proteins and nanotubes, *E. coli* strains and plasmids used in this study, DNA manipulations, protein expression, and purification (PDF)

■ AUTHOR INFORMATION

Corresponding Author

*E-mail: baneyx@uw.edu.

ORCID

François Baneyx: 0000-0001-5596-7903

Notes

The authors declare the following competing financial interest(s): F.B. declares competing financial interest in Proteios which researches and commercializes Car9-based technologies.

■ ACKNOWLEDGMENTS

This work was supported by the U.S. Office of Naval Research through award BRC-11123566. Partial support for SEM and TEM imaging of hybrid nanostructures was provided by the U.S. Department of Energy, Office of Science, Office of Basic Energy Sciences, as part of the Energy Frontier Research Centers program: CSSAS, Center for the Science of Synthesis Across Scales under Award Number DE-SC0019288. SEM and TEM imaging was conducted at the University of Washington Molecular Analysis Facility, a member of the NSF National Nanotechnology Coordinated Infrastructure (NNCI). We are

DOI: 10.1021/acs.bioconjchem.9b00097
Bioconjugate Chem. 2019, 30, 959−965

grateful to Gizem Gökçe for contributing to initial nanotube resuspension experiments.

REFERENCES

(1) Bernholc, J., Brenner, D., Nardelli, M. B., Meunier, V., and Roland, C. (2002) Mechanical and electrical properties of nanotubes. *Annu. Rev. Mater. Res. 32*, 347−375.
(2) Odom, T. W., Huang, J.-L., Kim, P., and Lieber, C. M. (1998) Atomic structure and electronic properties of single-walled carbon nanotubes. *Nature 391*, 62−64.
(3) Qian, H., Greenhalgh, E. S., Shaffer, M. S. P., and Bismarck, A. (2010) Carbon nanotube-based hierarchical composites: A review. *J. Mater. Chem. 20*, 4751−4762.
(4) Baptista, F. R., Belhout, S. A., Giordani, S., and Quinn, S. J. (2015) Recent developments in carbon nanomaterial sensors. *Chem. Soc. Rev. 44*, 4433−4453.
(5) Rosi, N. L., and Mirkin, C. A. (2005) Nanostructures in biodiagnostics. *Chem. Rev. 105*, 1547−1562.
(6) Yum, K., Ahn, J. H., McNicholas, T. P., Barone, P. W., Mu, B., Kim, J. H., Jain, R. M., and Strano, M. S. (2012) Boronic acid library for selective, reversible near-infrared fluorescence quenching of surfactant suspended single-walled carbon nanotubes in response to glucose. *ACS Nano 6*, 819−830.
(7) Calvaresi, M., and Zerbetto, F. (2013) The devil and holy water: Protein and carbon nanotube hybrids. *Acc. Chem. Res. 46*, 2454−2463.
(8) Allen, B. L., Kichambare, P. D., and Star, A. (2007) Carbon nanotube field-effect-transistor-based biosensors. *Adv. Mater. 19*, 1439−1451.
(9) Bradley, K., Briman, M., Star, A., and Gruner, G. (2004) Charge transfer from adsorbed proteins. *Nano Lett. 4*, 253−256.
(10) Karousis, N., Tagmatarchis, N., and Tasis, D. (2010) Current progress on the chemical modification of carbon nanotubes. *Chem. Rev. 110*, 5366−5397.
(11) Hirsch, A. (2002) Functionalization of single-walled carbon nanotubes. *Angew. Chem., Int. Ed. 41*, 1853−1859.
(12) Antonucci, A., Kupis-Rozmyslowicz, J., and Boghossian, A. A. (2017) Noncovalent protein and peptide functionalization of single-walled carbon nanotubes for biodelivery and optical sensing applications. *ACS Appl. Mater. Interfaces 9*, 11321−11331.
(13) Karajanagi, S. S., Vertegel, A. A., Kane, R. S., and Dordick, J. S. (2004) Structure and function of enzymes adsorbed onto single-walled carbon nanotubes. *Langmuir 20*, 11594−11599.
(14) Kurppa, K., Jiang, H., Szilvay, G. R., Nasibulin, A. G., Kauppinen, E. L., and Linder, M. B. (2007) Controlled hybrid nanostructures through protein-mediated noncovalent functionalization of carbon nanotube. *Angew. Chem., Int. Ed. 46*, 6446−6449.
(15) Matsuura, K., Saito, T., Okazaki, T., Ohshima, S., Yumura, M., and Iijima, S. (2006) Selectivity of water-soluble proteins in single-walled carbon nanotube dispersions. *Chem. Phys. Lett. 429*, 497−502.
(16) Liu, P. (2005) Modifications of carbon nanotubes with polymers. *Eur. Polym. J. 41*, 2693−2703.
(17) Welsher, K., Liu, Z., Sherlock, S. P., Robinson, J. T., Chen, Z., Daranciang, D., and Dai, H. J. (2009) A route to brightly fluorescent carbon nanotubes for near-infrared imaging in mice. *Nat. Nanotechnol. 4*, 773−780.
(18) Hertel, T., Hagen, A., Talalaev, V., Arnold, K., Hennrich, F., Kappes, M., Rosenthal, S., McBride, J., Ulbricht, H., and Flahaut, E. (2005) Spectroscopy of single- and double-wall carbon nanotubes in different environments. *Nano Lett. 5*, 511−514.
(19) Bergler, F. F., Stahl, S., Goy, A., Schoppler, F., and Hertel, T. (2016) Substrate-mediated cooperative adsorption of sodium cholate on (6,5) single-wall carbon nanotubes. *Langmuir 32*, 9598−9603.
(20) Zhao, Y. L., and Stoddart, J. F. (2009) Noncovalent functionalization of single-walled carbon nanotubes. *Acc. Chem. Res. 42*, 1161−1171.
(21) Dai, H. J. (2002) Carbon nanotubes: Synthesis, integration, and properties. *Acc. Chem. Res. 35*, 1035−1044.
(22) Oliveira, S. F., Bisker, G., Bakh, N. A., Gibbs, S. L., Landry, M. P., and Strano, M. S. (2015) Protein functionalized carbon nanomaterials for biomedical applications. *Carbon 95*, 767−779.
(23) Sarikaya, M., Tamerler, C., Jen, A. K., Schulten, K., and Baneyx, F. (2003) Molecular biomimetics: Nanotechnology through biology. *Nat. Mater. 2*, 577−585.
(24) Lee, Y. J., Yi, H., Kim, W. J., Kang, K., Yun, D. S., Strano, M. S., Ceder, G., and Belcher, A. M. (2009) Fabricating genetically engineered high-power lithium-ion batteries using multiple virus genes. *Science 324*, 1051−1055.
(25) Pender, M. J., Sowards, L. A., Hartgerink, J. D., Stone, M. O., and Naik, R. R. (2006) Peptide-mediated formation of single-wall carbon nanotube composites. *Nano Lett. 6*, 40−44.
(26) Su, Z. D., Leung, T., and Honek, J. F. (2006) Conformational selectivity of peptides for single-walled carbon nanotubes. *J. Phys. Chem. B 110*, 23623−23627.
(27) Wang, S., Humphreys, E. S., Chung, S.-Y., Delduco, D. F., Lustig, S. R., Wang, H., Parker, K. N., Rizzo, N. W., Subramoney, S., Chiang, Y.-M., et al. (2003) Peptides with selective affinity for carbon nanotubes. *Nat. Mater. 2*, 196−200.
(28) Zheng, L. F., Jain, D., and Burke, P. (2009) Nanotube-peptide interactions on a silicon chip. *J. Phys. Chem. C 113*, 3978−3985.
(29) Inou, I., Zheng, B., Watanabe, K., Ishikawa, Y., Shiba, K., Yasueda, H., Uraoka, Y., and Yamashita, I. (2011) A novel bifunctional protein supramolecule for construction of carbon nanotube-titanium hybrid material. *Chem. Commun. 47*, 12649−12651.
(30) Coyle, B. L., Rolandi, M., and Baneyx, F. (2013) Carbon-binding designer proteins that discriminate between sp^2- and sp^3-hybridized carbon surfaces. *Langmuir 29*, 4839−4846.
(31) Coyle, B. L., and Baneyx, F. (2016) Direct and reversible immobilization and microcontact printing of functional proteins on glass using a genetically appended silica-binding tag. *Chem. Commun. 52*, 7001−7004.
(32) Yang, W., Hellner, B., and Baneyx, F. (2016) Self-immobilization of Car9 fusion proteins within high surface area silica sol-gels and dynamic control of protein release. *Bioconjugate Chem. 27*, 2450−2459.
(33) Coyle, B. L., and Baneyx, F. (2014) A cleavable silica-binding affinity tag for rapid and inexpensive protein purification. *Biotechnol. Bioeng. 111*, 2019−2026.
(34) Soto-Rodriguez, J., Coyle, B. L., Samuelson, A., Aravagiri, K., and Baneyx, F. (2017) Affinity purification of Car9-tagged proteins on silica matrices: Optimization of a rapid and inexpensive protein purification technology. *Protein Expression Purif. 135*, 70−77.
(35) Pedelacq, J. D., Cabantous, S., Tran, T., Terwilliger, T. C., and Waldo, G. S. (2006) Engineering and characterization of a superfolder green fluorescent protein. *Nat. Biotechnol. 24*, 79−88.
(36) Shaner, N. C., Campbell, R. E., Steinbach, P. A., Giepmans, B. N. G., Palmer, A. E., and Tsien, R. Y. (2004) Improved monomeric red, orange and yellow fluorescent proteins derived from *Discosoma* sp. Red fluorescent protein. *Nat. Biotechnol. 22*, 1567−1572.
(37) Inam, F., Reece, M. J., and Peijs, T. (2012) Shortened carbon nanotubes and their influence on the electrical properties of polymer nanocomposites. *J. Compos. Mater. 46*, 1313−1322.
(38) Lu, K. L., Lago, R. M., Chen, Y. K., Green, M. L. H., Harris, P. J. F., and Tsang, S. C. (1996) Mechanical damage of carbon nanotubes by ultrasound. *Carbon 34*, 814−816.
(39) Crowe, J., Masone, B. S., and Ribbe, J. (1995) One-step purification of recombinant proteins with the 6xhis tag and Ni-NTA resin. *Mol. Biotechnol. 4*, 247−258.
(40) Naik, R. R., Stringer, S. J., Agarwal, G., Jones, S. E., and Stone, M. O. (2002) Biomimetic synthesis and patterning of silver nanoparticles. *Nat. Mater. 1*, 169−172.
(41) Thomas, A., Matthaei, J. F., and Baneyx, F. (2018) A self-assembling two-dimensional protein array is a versatile platform for the assembly of multicomponent nanostructures. *Biotechnol. J. 13*, No. 1800141.

DOI: 10.1021/acs.bioconjchem.9b00097
Bioconjugate Chem. 2019, 30, 959−965

(42) Swift, B. J., Shadish, J. A., DeForest, C. A., and Baneyx, F. (2017) Streamlined synthesis and assembly of a hybrid sensing architecture with solid binding proteins and click chemistry. *J. Am. Chem. Soc. 139*, 3958−3961.
(43) Uvdal, K., Bodo, P., and Liedberg, B. (1992) L-cysteine adsorbed on gold and copper - an x-ray photoelectron-spectroscopy study. *J. Colloid Interface Sci. 149*, 162−173.

DOI: 10.1021/acs.bioconjchem.9b00097
Bioconjugate Chem. 2019, 30, 959−965